SIAM J. SCI. COMPUT.
Vol. 22, No. 6, pp. 2152–2177

A SEMI-LAGRANGIAN FINITE VOLUME METHOD FOR NEWTONIAN CONTRACTION FLOWS *

T. N. PHILLIPS† AND A. J. WILLIAMS‡

Abstract. A new finite volume method for solving the incompressible Navier–Stokes equations is presented. The main features of this method are the location of the velocity components and pressure on different staggered grids and a semi-Lagrangian method for the treatment of convection. An interpolation procedure based on area-weighting is used for the convection part of the computation. The method is applied to flow through a constricted channel, and results are obtained for Reynolds numbers, based on half the flow rate, up to 1000. The behavior of the vortex in the salient corner is investigated qualitatively and quantitatively, and excellent agreement is found with the numerical results of Dennis and Smith [*Proc. Roy. Soc. London A*, 372 (1980), pp. 393–414] and the asymptotic theory of Smith [*J. Fluid Mech.*, 90 (1979), pp. 725–754].

Key words. semi-Lagrangian approach, Navier–Stokes, finite volume method, contraction geometry, staggered mesh, SIMPLER algorithm

AMS subject classifications. 65N06, 65N22, 76D05, 76M25

PII. S1064827599365288

1. Introduction.

In this paper a semi-Lagrangian finite volume method is presented for solving incompressible flows of Newtonian fluids. This approach is shown to be particularly well suited to solving the Navier–Stokes equations for which the discretization of the governing equations is well known to be crucial when the flow is convection dominated. Numerical difficulties can occur for large values of the Reynolds number, a nondimensional quantity which measures the relative importance of convection compared to diffusion. Central difference schemes, which perform well for low Reynolds number flows, are prone to numerical difficulties for higher Reynolds numbers. For low Reynolds numbers central difference schemes produce a diagonally dominant system of equations which can be solved without any difficulty using standard relaxation techniques. At higher Reynolds numbers diagonal dominance is lost with the result that one can encounter problems using the same schemes. These difficulties can manifest themselves in several ways. For example, relaxation techniques may fail to converge, and if a solution is obtained for the steady problem, it may exhibit physically unrealistic oscillations.

A popular finite volume approach for overcoming the difficulties associated with the treatment of convection uses interpolation biased towards the upwind direction when the flow is convection dominated. Low-order interpolation invariably results in artificial or false diffusion being added to the scheme. The effect of this is a degradation in accuracy. Higher-order interpolation schemes such as quadratic upwind interpolation for convection kinematics (QUICK) [6] and SMART [9] increase the complexity of the scheme and create difficulties near boundaries. In the presence of high gradients, they may additionally produce overshoot or undershoot values. Nonlinear flux limiting functions may be used in conjunction with high-order upwinding

*Received by the editors January 5, 2000; accepted for publication (in revised form) November 8, 2000; published electronically April 26, 2001.
http://www.siam.org/journals/sisc/22-6/36528.html
†Department of Mathematics, University of Wales, Aberystwyth SY23 3BZ, UK (tnp@aber.ac.uk).
‡Department of Mathematics, University of Wales, Aberystwyth SY23 3BZ, United Kingdom. Present address: School of Computing and Mathematical Sciences, University of Greenwich, London SE10 9LS, United Kingdom (A.J.Williams@greenwich.ac.uk)

techniques to prevent the appearance of over- or undershoots. The underlying idea behind these techniques is to control the gradients of the computed solution through the use of total variation diminishing schemes (TVD) schemes (see Hirsch [1] for a comprehensive review of this subject). It is the treatment of convection together with the positioning of the mesh points that distinguish one finite volume method from another.

In time-dependent calculations standard finite volume schemes possess time-step restrictions due to stability. These may be more severe than the conditions imposed by accuracy considerations alone. When particle following techniques are used the stability conditions are much less restrictive. However, the unrestricted movement of the points used in Lagrangian methods, which involves following a fixed set of particles throughout the flow, introduces other difficulties. For example, a set of fluid particles which is initially regularly distributed soon becomes greatly deformed, in general, and is thus rendered unsuitable for numerical integration. Semi-Lagrangian methods avoid this difficulty while still following particles. A semi-Lagrangian method for treating the convection term, in which particles on a regular grid of points are traced backwards over a single time-step to their departure points, provides the focus of this paper. Although semi-Lagrangian finite volume methods have been developed for advection problems [22, 24, 25], this paper describes their application to problems in Newtonian computational fluid dynamics. This scheme circumvents the problems associated with upwind biased interpolation schemes, possesses less restrictive stability requirements, and combines the advantages of fixed grids inherent in Eulerian methods with modifications to the location of grid points at previous time-steps based on the Lagrangian approach.

The remaining terms in the governing equations are treated implicitly and are discretized by integrating over an appropriate control volume. The discrete equations are solved using the semi-implicit method for pressure linked equations revised (SIMPLER) [19] algorithm. Therefore, this approach may be viewed as a time-splitting scheme in which the different operators in the governing equations are discretized by appropriate techniques.

The emphasis in this paper is on the semi-Lagrangian treatment of convection. This can only be accomplished within the framework of time-splitting schemes for time-dependent problems. Therefore, the proposed semi-Lagrangian finite volume method is described for time-dependent problems even though, in this paper, it is only used as a means of reaching the steady state solution. The temporal accuracy of the scheme depends on the discretization of the characteristic paths as well as the temporal discretization of the governing equations. Since a first-order scheme is used for the latter, there is no advantage in using a higher-order scheme for the characteristic calculation. The development of high-order discretizations for all the component parts of the proposed scheme is an area of ongoing activity.

The important features of the method are illustrated on a pure convection problem before it is applied to the flow through an abruptly contracting channel in which the ratio of the channel widths before and after the contraction is 2:1. Numerical results are presented for Reynolds numbers in the range [0,1000]. The behavior of the vortex in the salient corner is investigated, and comparisons are made with other results in the literature. Smith [12] developed an asymptotic theory for the flow upstream of the contraction. Good agreement is shown with this theory for the location of the upstream separation point for Reynolds numbers greater than about 100. The size of the salient corner vortex decreases as the Reynolds number increases from 0 to around

50. As the Reynolds number is increased further, the vortex grows slowly.

This paper is organized as follows. In section 2 the governing equations and flow geometry are described. The location of the dependent variables on a staggered grid and the conventional finite volume discretization of the governing equations are described in section 3. In section 4 we describe the semi-Lagrangian treatment of the convection terms. In section 5 we show how this is incorporated into a solution procedure for solving the Navier–Stokes equations based on the SIMPLER algorithm. Numerical results and comparisons with other work are presented in section 6. Finally, concluding remarks are made in section 7.

2. Governing equations. We consider the laminar flow of an incompressible fluid of viscosity η through an abruptly contracting channel with walls at $y = \pm 1$ for $x < 0$, $y = \pm\frac{1}{2}$ for $x > 0$, and $\frac{1}{2} \leq |y| \leq 1$ for $x = 0$. A schematic diagram of the lower half of this geometry is shown in Figure 1. Upstream of the contraction we impose parabolic Poiseuille flow, and we suppose that the flow is parabolic again far enough downstream. Since the flow is symmetric about $y = 0$, it is only necessary to seek a solution for $y \leq 0$.

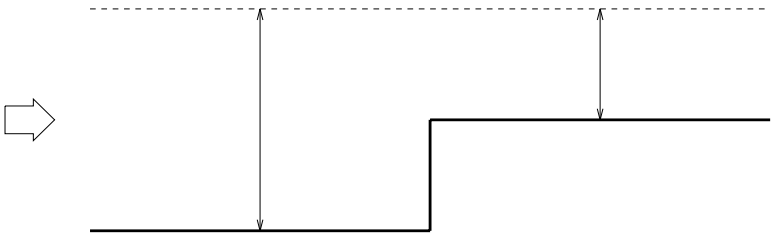

FIG. 1. *Geometry for the* 2:1 *planar contraction.*

The time-dependent Navier–Stokes equations are

$$\rho\left[\frac{\partial \boldsymbol{u}}{\partial t} + \boldsymbol{u}.\nabla\boldsymbol{u}\right] = \eta\nabla^2\boldsymbol{u} - \nabla p, \tag{2.1}$$

$$\nabla.\boldsymbol{u} = 0, \tag{2.2}$$

where $\boldsymbol{u} = (u, v)$ is the velocity vector, p is the pressure, and ρ is the density. Nondimensional quantities are defined as

$$\boldsymbol{x}^* = \frac{\boldsymbol{x}}{L}, \quad t^* = \frac{Ut}{L}, \quad \boldsymbol{u}^* = \frac{\boldsymbol{u}}{U}, \quad p^* = \frac{p}{\rho U^2},$$

where U is a characteristic flow speed and L is a characteristic length scale of the flow. With the Reynolds number, Re, defined by

$$Re = \frac{\rho U L}{\eta},$$

we may write the Navier–Stokes equations in dimensionless form. In two-dimensional

component form they are

$$\frac{\partial u}{\partial t} + u\frac{\partial u}{\partial x} + v\frac{\partial u}{\partial y} = \frac{1}{Re}\left[\frac{\partial^2 u}{\partial x^2} + \frac{\partial^2 u}{\partial y^2}\right] - \frac{\partial p}{\partial x}, \tag{2.3}$$

$$\frac{\partial v}{\partial t} + u\frac{\partial v}{\partial x} + v\frac{\partial v}{\partial y} = \frac{1}{Re}\left[\frac{\partial^2 v}{\partial x^2} + \frac{\partial^2 v}{\partial y^2}\right] - \frac{\partial p}{\partial y}, \tag{2.4}$$

$$\frac{\partial u}{\partial x} + \frac{\partial v}{\partial y} = 0, \tag{2.5}$$

where we have dropped the $*$ notation for ease of notation.

For the contraction problem the characteristic length scale (L) is chosen to be the downstream half-channel width, and the characteristic flow speed (U) is chosen to be the mean velocity across half of the downstream channel. Therefore, the boundary conditions are given by

$$\boldsymbol{u} = 0 \quad \text{on} \quad y = \begin{cases} -1 & \text{for } x \le 0, \\ -\frac{1}{2} & \text{for } x \ge 0, \end{cases}$$

$$\boldsymbol{u} = 0 \quad \text{on} \quad x = 0 \text{ for } -1 \le y \le -\frac{1}{2},$$

$$v = 0, \frac{\partial u}{\partial y} = 0 \quad \text{on} \quad y = 0,$$

$$u \to \frac{3}{2}(1 - y^2),\ v \to 0 \quad \text{as} \quad x \to -\infty,$$

$$u \to 3(1 - 4y^2),\ v \to 0 \quad \text{as} \quad x \to \infty.$$

3. Finite volume discretization. The finite volume method is generally applied to a system of differential equations written in conservation form, e.g.,

$$\frac{\partial \boldsymbol{w}}{\partial t} + \frac{\partial \boldsymbol{f}}{\partial x} + \frac{\partial \boldsymbol{g}}{\partial y} = \boldsymbol{S}, \tag{3.1}$$

where $\boldsymbol{w}$ is the vector of unknowns, $\boldsymbol{f}$ and $\boldsymbol{g}$ are vector functions of $\boldsymbol{x} = (x, y)$, $\boldsymbol{w}$, and $\nabla \boldsymbol{w}$, and $\boldsymbol{S}$ is the source term. In this paper we consider cell center finite volume methods. These methods are closely related to finite difference methods.

A grid is placed on the computational domain, and a control or finite volume is associated with each unknown on the grid. Each component equation of (3.1) is integrated over the appropriate control volume. Finite difference type approximations are then used to approximate line integrals over each side of the control volume. There is a number of ways of doing this, each leading to a numerical scheme satisfying certain properties. In the finite volume formulation mass and momentum are conserved over every control volume and therefore over the whole computational domain. The property of conservation of physical quantities, which is preserved by the discrete system, is one of the attractions and advantages of the finite volume method.

A staggered grid is used in which the different dependent variables are approximated at different mesh points (see Figure 2). This type of mesh arrangement ensures that the solution is not polluted by spurious pressure modes. On a nonstaggered mesh the familiar checkerboard mode is present.

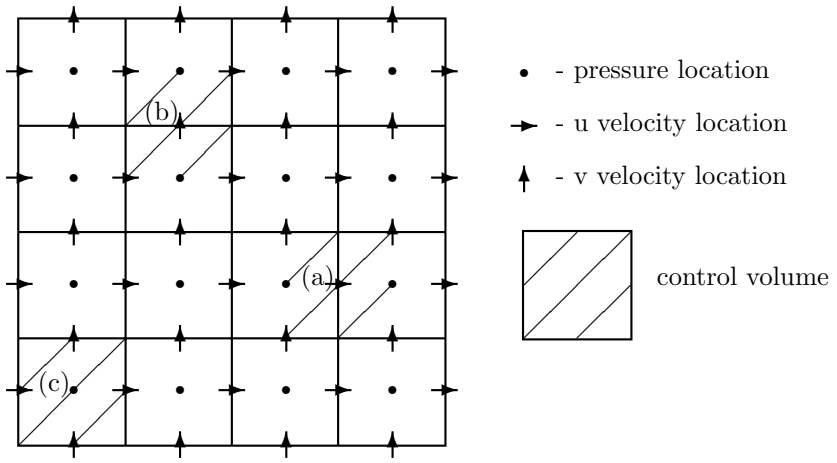

FIG. 2. *A staggered grid depicting the control volumes for* (a) *u-momentum equation,* (b) *v-momentum equation, and* (c) *continuity equation.*

TABLE 1
Definition of the symbols in the general equation (3.2).

Equation	ϕ	δ	Γ	S_ϕ
u-momentum	u	1	$(Re)^{-1}$	$-\frac{\partial p}{\partial x}$
v-momentum	v	1	$(Re)^{-1}$	$-\frac{\partial p}{\partial y}$
continuity	1	0	0	0

Each of the governing equations (2.3)–(2.5) can be cast into the general conservative form

$$\delta\frac{\partial\phi}{\partial t}+\frac{\partial}{\partial x}\left(u\phi-\Gamma\frac{\partial\phi}{\partial x}\right)+\frac{\partial}{\partial y}\left(v\phi-\Gamma\frac{\partial\phi}{\partial y}\right)=S_\phi, \tag{3.2}$$

where δ and Γ are constants and ϕ and S_ϕ are functions that are defined depending on the particular equation under consideration (see Table 1).

Equation (3.2) is discretized in time using the backward Euler method with time-step Δt to give

$$\frac{\partial}{\partial x}\left(u\phi^{n+1}-\Gamma\frac{\partial\phi^{n+1}}{\partial x}\right)+\frac{\partial}{\partial y}\left(u\phi^{n+1}-\Gamma\frac{\partial\phi^{n+1}}{\partial y}\right)=S_\phi^{n+1}-\frac{\delta}{\Delta t}(\phi^{n+1}-\phi^n), \tag{3.3}$$

where ϕ^{n+1} denotes the approximation to the variable ϕ at the $(n+1)$th time-step. Note that this semidiscrete scheme can be used as the basis for determining solutions to transient or steady problems.

The finite volume methodology proceeds by integrating (3.3) over a control volume

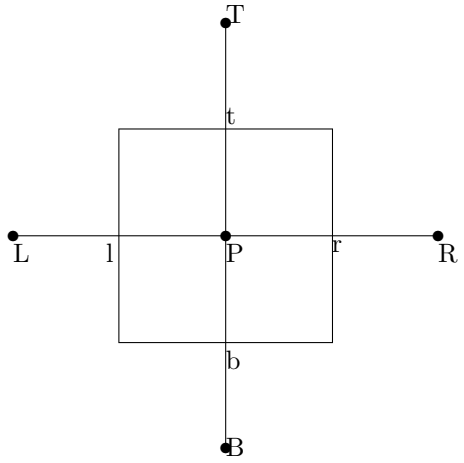

FIG. 3. *A general control volume.*

(see Figure 3, for example) and using the divergence theorem. This yields the equation

$$\begin{aligned}\int_b^t \left[\left(u\phi^{n+1} - \Gamma\frac{\partial\phi^{n+1}}{\partial x}\right)_r - \left(u\phi^{n+1} - \Gamma\frac{\partial\phi^{n+1}}{\partial x}\right)_l\right] dy \\ + \int_l^r \left[\left(v\phi^{n+1} - \Gamma\frac{\partial\phi^{n+1}}{\partial y}\right)_t - \left(v\phi^{n+1} - \Gamma\frac{\partial\phi^{n+1}}{\partial y}\right)_b\right] dx \\ = \int_b^t\int_l^r \left[S_\phi^{n+1} - \frac{\delta}{\Delta t}(\phi^{n+1} - \phi^n)\right] dxdy. \end{aligned} \tag{3.4}$$

Each of the integral terms on the left-hand side of (3.4) represents a transport by convection and diffusion through the relevant control-volume face. All schemes use central differences to approximate the diffusive flux across each face. For example, across the vertical face passing through the point r we have

$$\left(\frac{\partial\phi}{\partial x}\right)_r \simeq \frac{\phi_R - \phi_P}{\Delta x}. \tag{3.5}$$

It is the approximation of the convective flux which differentiates one finite volume scheme from another. We shall review briefly some of the common approaches, many of which are based on some form of upwinding to retain accuracy and stability when convection dominates diffusion.

A central difference approximation to the convective flux would take the form

$$(u\phi^{n+1})_r \simeq u_r^n \frac{(\phi_R^{n+1} + \phi_P^{n+1})}{2}, \tag{3.6}$$

for example. Note that the velocity component u is frozen at its value from the previous time-step. In steady calculations it would be frozen at its value from the previous iteration since iterative methods are generally used to solve the algebraic equation resulting from a finite volume discretization. Therefore, in the case of the u-momentum equation, we arrive at the discretization

$$\begin{aligned} A_P u_P^{n+1} = A_R u_R^{n+1} + A_L u_L^{n+1} + A_T u_T^{n+1} + A_B u_B^{n+1} \\ + \frac{u_P^n \Delta x \Delta y}{\Delta t} + (p_l^{n+1} - p_r^{n+1})\Delta y, \end{aligned} \tag{3.7}$$

where

$$A_R = -\frac{F_r}{2} + D_r,$$
$$A_L = \frac{F_l}{2} + D_l,$$
$$A_T = -\frac{F_t}{2} + D_t,$$
$$A_B = \frac{F_b}{2} + D_b,$$
$$A_P = A_R + A_L + A_T + A_B + F_r - F_l + F_t - F_b + \frac{\Delta x \Delta y}{\Delta t}, \tag{3.8}$$

and $F_r = u_r^n \Delta y$, $D_r = \frac{1}{Re}\frac{\Delta y}{\Delta x}$, etc.

The local truncation error for the central-difference approximation is second-order. An essential requirement for a bounded solution is that all the coefficients A_{nb}, where the subscript nb refers to the neighbors of P, should be of the same sign, usually all positive. If the resulting system of equations is diagonally dominant, then many of the standard iterative methods can be used, and convergence is guaranteed. This property is assured, and oscillatory solutions arising from negative roots to the characteristic equation are prevented, if the following conditions are satisfied:

$$A_{nb} > 0 \quad \text{and} \quad A_P \geq -(A_R + A_L + A_T + A_B). \tag{3.9}$$

However, looking at the coefficients given in (3.8), we see that in some circumstances some coefficients A_{nb} may become negative. Thus for convergence to be guaranteed we require the mesh Peclet number given by

$$Pe = \frac{F}{D},$$

where $F = u\Delta y$ and $D = \frac{1}{Re}\frac{\Delta y}{\Delta x}$, to be less than 2 in order to satisfy this boundedness criterion, i.e.,

$$u\, Re \Delta x < 2,$$

or

$$\Delta x < \frac{2}{u\, Re}. \tag{3.10}$$

Similarly, we also require

$$\Delta y < \frac{2}{v\, Re}. \tag{3.11}$$

For $Pe > 2$ the scheme may converge but to physically unrealistic solutions. This means that the central-difference method is limited to low values of Re unless the mesh is suitably refined so that conditions (3.10) and (3.11) are satisfied. Since this would be computationally expensive, the central-difference technique is not suitable for convection-dominated flow problems.

From a physical point of view central difference schemes are not suitable for convection dominated problems because the direction of the flow is not used in the derivation of the approximation. The upwind scheme takes this into account and

proposes that the value of u at the interface is equal to the value of u at the grid point on the upwind side of the face, i.e.,

$$u_r^{n+1} = \begin{cases} u_P^{n+1} & \text{if } u_r^n > 0, \\ u_R^{n+1} & \text{if } u_r^n < 0. \end{cases} \tag{3.12}$$

This approximation again leads to an equation of the form (3.7), but now the coefficients satisfy the boundedness criterion (3.9) for all Reynolds numbers. The local truncation error for the upwind scheme is first order. Since the upwind scheme is simple to use, it has been widely applied in applications in computational fluid dynamics. It is easily extended to three-dimensional problems. However, a major drawback with the scheme is that it causes the distribution of the transported properties to become smeared, particularly when the flow is not aligned with the grid lines. The error has a diffusion-like appearance and is referred to as artificial diffusion. Refinement of the grid can overcome this problem, but it is expensive. At high Reynolds numbers the error due to artificial diffusion can be large enough to give physically incorrect results.

In an attempt to reduce the amount of false diffusion present in the simple upwind scheme and to improve the overall accuracy of the finite volume scheme Leonard [6] introduced the QUICK scheme to approximate the convective fluxes. This scheme is based on the use of a second degree polynomial biased toward the upstream direction to interpolate the value of the dependent variable, u_r, at each face of the control volume.

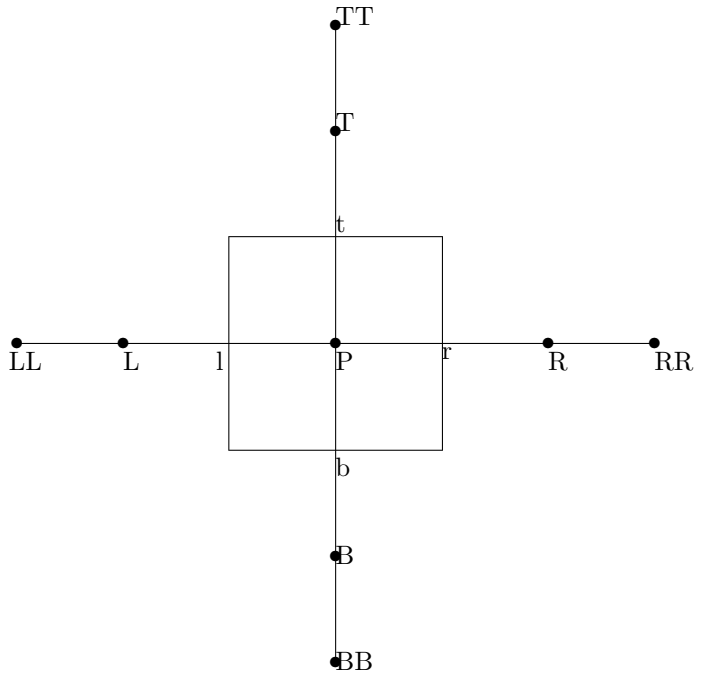

FIG. 4. *A control volume for use with the QUICK scheme.*

This leads to a third order approximation possessing a larger stencil as shown in Figure 4. A drawback of the scheme is that the coefficients corresponding to points R, L, T, and B are not guaranteed to be positive and the coefficients corresponding to points RR, LL, TT, and BB are negative. Thus the QUICK scheme is only

conditionally stable, and there is a tendency for QUICK to give oscillatory results. Furthermore, the conversion of this method to a three-dimensional scheme is likely to cause more difficulties than the upwind method due to the extra terms in the momentum equations.

In this paper we have pursued an entirely different approach to the treatment of convection. Instead of using upwinding to stabilize the scheme at moderate values of the Reynolds number, we have chosen to treat convection in a semi-Lagrangian manner. This is described in the next section.

4. A semi-Lagrangian approach. The underlying problem with the traditional finite volume treatment of convection diffusion problems is that the convection term is discretized using what is essentially a technique that has been constructed and tested for diffusion problems. Upwinding attempts to redress the situation as far as convection is concerned by giving some weighting to the convection part of the problem. The approach adopted in this paper is a time-splitting technique in which we decouple the treatment of convection and diffusion and use appropriate methods of discretization for each subproblem. Over each time interval $[t_n, t_{n+1}]$ we solve a convection equation of the form

$$\frac{\partial \boldsymbol{u}}{\partial t} + \boldsymbol{u}^n.\nabla \boldsymbol{u} = 0, \tag{4.1}$$

followed by the solution of an unsteady generalized Stokes problem

$$\frac{\partial \boldsymbol{u}}{\partial t} - \frac{1}{Re}\nabla^2 \boldsymbol{u} + \nabla p = 0, \tag{4.2}$$

$$\nabla.\boldsymbol{u} = 0. \tag{4.3}$$

The natural frame of reference in which to solve (4.1) is defined by the particle following transformation

$$\begin{aligned} \frac{d\xi(t)}{dt} &= u^n(\xi(t), \eta(t), \tau), \\ \frac{d\eta(t)}{dt} &= v^n(\xi(t), \eta(t), \tau), \\ \frac{d\tau(t)}{dt} &= 1, \end{aligned} \tag{4.4}$$

where ξ and η are the spatial variables and τ is the temporal variable. For $\mathbf{x} = (x, y) \in \mathrm{R}^2$ the solution of the system of ordinary differential equations (4.4) for $t \in [t_n, t_{n+1}]$ subject to

$$\xi(t_{n+1}) = x, \quad \eta(t_{n+1}) = y, \quad \tau(t_{n+1}) = t_{n+1}, \tag{4.5}$$

is a continuous curve, known as the trajectory, in space-time passing through the point (x, y, t_{n+1}). After applying a transformation which satisfies (4.4), the governing equation for $\mathbf{u}$ becomes

$$\frac{d\mathbf{u}}{d\tau}(\xi, \eta, \tau) = 0. \tag{4.6}$$

Thus smooth solutions of (4.1) are constant along the characteristic paths [18].

In this section we concentrate on the novel features of our finite volume scheme which is the discretization of (4.1) using a semi-Lagrangian approach. This approach

differs from that proposed by Manson and Wallis [25]. The scheme of Manson and Wallis [25] was developed for pure advection problems in one dimension and is based on a fractional-staged strategy that combines a conventional control volume discretization over a partial time-step $\tau\Delta t$ $(0 < \tau < 1)$ with a semi-Lagrangian treatment over the partial time-step $(1-\tau)\Delta t$. The value of τ is chosen to avoid the need for interpolation in the semi-Lagrangian part of the calculation. The solution of (4.2) and (4.3) follows standard finite volume methodology. The discrete formulation of this problem can be solved using the SIMPLER approach, for example.

The computational domain is partitioned into a number of nonoverlapping control volumes or cells, $C_{i,j}$. This grid, known as the reference grid, remains fixed in space for all time. Consider the mesh associated with one of the dependent variables, ϕ, say, where $\phi = u$ or v. Let $C_{i,j}$ be one such control volume. Let the positions of the corners of cell $C_{i,j}$ be located at the points $\mathbf{X}_{i\pm1/2,j\pm1/2} = (x_{i\pm1/2}, y_{j\pm1/2})$. Particles which arrive at these four corner points at time $t = t_{n+1}$ were located at the vertices of some cell, which is to be determined as part of the solution process, at time $t = t_n$. In general, this will be a deformed control volume which may lie anywhere on the underlying grid or indeed outside the domain if the time-step is sufficiently large. We approximate this cell by a quadrilateral $C^{*n}_{i,j}$, formed by joining the departure points by straight line segments.

Associated with each cell $C_{i,j}$ at each time $t_n = n\Delta t$ an approximation is introduced, denoted by $\bar{\phi}^n_{i,j}$, to the cell average of $\phi(x, y, t_n)$, i.e.,

$$\phi^n_{i,j} \approx \frac{1}{\Delta x_i \Delta y_j} \iint_{C_{i,j}} \phi(x, y, t_n)\, dxdy, \tag{4.7}$$

where

$$\Delta x_i = x_{i+1/2} - x_{i-1/2}, \quad \Delta y_j = y_{j+1/2} - y_{j-1/2}.$$

Note that $\phi^n_{i,j}$ will, in general, be distinct from the pointwise approximation to $\phi(x_i, y_j, t_n)$.

An approximation to the solution of (4.1) is given by

$$\bar{\phi}^{n+1}_{i,j} = \bar{\phi}^{*n}_{i,j}, \tag{4.8}$$

where

$$\bar{\phi}^{*n}_{i,j} \approx \frac{1}{\Delta x_i \Delta y_j} \iint_{C^{*n}_{i,j}} \phi(x, y, t_n)\, dxdy. \tag{4.9}$$

Thus there are two stages to the numerical calculation at each time-step. In the first stage the departure points are determined. These are the vertices of the cells $C^{*n}_{i,j}$. In the second stage the cell average values of ϕ^{*n} are determined from a knowledge of the cell average values of ϕ at time $t = t_n$ on the reference grid. These values are then inserted into the discretized versions of equations (4.2) and (4.3) in order to determine the values of velocity and pressure at the new time-step.

4.1. Calculation of departure points. The departure points at time t_n of each point on the reference grid are determined by solving the particle following transformation (4.4) for $t \in [t_n, t_{n+1}]$, subject to

$$\xi(t_{n+1}) = x_{i+\frac{1}{2},j+\frac{1}{2}}, \quad \eta(t_{n+1}) = y_{i+\frac{1}{2},j+\frac{1}{2}}, \quad \tau(t_{n+1}) = t_{n+1}. \tag{4.10}$$

This computation is performed for each grid point, i.e., for a suitable range of values of i and j in (4.10). The solution of this problem describes the path of the particle that passes through the grid point

$$\mathbf{X}_{i+\frac{1}{2},j+\frac{1}{2}} = (x_{i+\frac{1}{2},j+\frac{1}{2}}, y_{i+\frac{1}{2},j+\frac{1}{2}})$$

at time $t = t_{n+1}$. Each of these paths is traced backwards in time over one time-step. For example, if $C_{i,j}$ represents a control volume for the u component of velocity, then the following one-step method may be used to determine the positions of the corners of $C^{*n}_{i,j}$:

$$\begin{aligned} x^{*n}_{i+\frac{1}{2},j+\frac{1}{2}} &= x^{n+1}_{i+\frac{1}{2},j+\frac{1}{2}} - \frac{\Delta t}{4}(u^n_{i,j} + u^n_{i+1,j} + u^n_{i,j+1} + u^n_{i+1,j+1}), \\ y^{*n}_{i+\frac{1}{2},j+\frac{1}{2}} &= y^{n+1}_{i+\frac{1}{2},j+\frac{1}{2}} - \Delta t v^n_{i+\frac{1}{2},j+\frac{1}{2}}, \end{aligned} \tag{4.11}$$

where subscripts indicate grid locations and superscripts indicate the time-step. The above scheme is first-order in time. Higher-order schemes in time may also be used.

4.2. Calculation of area-weighting coefficients. At the beginning of each time-step the values of $\phi^n_{i,j}$ are known in all control volumes. Given the location of the departure points of the reference grid at time t_n, the values $\phi^{*n}_{i,j}$ must be determined. This approximation is generated by means of an area-weighting technique which uses a weighted sum of the values of ϕ^n over the control volumes on the reference grid which overlap with cell $C^{*n}_{i,j}$. Area-weighting techniques are not new, and they have been demonstrated to possess attractive stability properties. They were originally developed by users of particle-in-cell methods [21, 20]. In the Lagrange–Galerkin finite element method the evaluation of inner products using nonexact integration must be performed with great care [3]. Large classes of well-known quadrature rules lead to conditionally unstable schemes. However, the use of area-weighting can restore the stability properties of the exactly integrated schemes, albeit with a slight degradation in accuracy. In the application of this technique the centroid of each element is tracked, and the whole element is deemed to move without distortion and rotation. However, in the present application of the technique the control volumes are allowed to move with distortion and rotation.

The first-order area-weighting scheme of Scroggs and Semazzi [4] for determining the value of $\phi^{*n}_{i,j}$ is

$$\phi^{*n}_{i,j} = \frac{1}{\Delta x_i \Delta y_j} \sum_{I,J \in Z} \omega^{I,J}_{i,j} \bar{\phi}^n_{I,J}, \tag{4.12}$$

where $\omega^{I,J}_{i,j}$ is the common area between $C^{*n}_{i,j}$ and $C_{I,J}$, i.e., the area of $C_{I,J} \cap C^{*n}_{i,j}$, and Z is the set of indices of all the points in the computational domain. This involves determining how the cell $C^{*n}_{i,j}$ intersects with the control volumes in the fixed grid at time t_n and then to perform an area weighting based on the amount of overlap. Although this procedure is a straightforward exercise in coordinate geometry, it requires careful programming. Details can be found in Williams [17]. This scheme possesses the important property that when it is applied to systems of conservation laws the numerical approximation preserves the discrete conservation property identically, i.e.,

$$\sum_{i,j \in Z} u^{*n}_{i,j} = \sum_{i,j \in Z} u^{n+1}, \tag{4.13}$$

if the boundaries of each control volume $C_{I,J}$ remain inside the computational domain from time t_n to t_{n+1} since

$$\sum_{i,j\in Z} \omega_{i,j}^{I,J} = \text{area of } C_{I,J}. \tag{4.14}$$

Higher-order extensions of this scheme have been derived by Phillips and Williams [16] and have been applied to conservation laws. In particular, Phillips and Williams [16] apply the first-order and higher-order schemes to a rotating disk test problem. The results which have been obtained fully demonstrate the conservation properties of all the schemes.

5. Stability and accuracy. In this section we investigate the stability and convergence properties of the semi-Lagrangian scheme on a pure convection problem in one space dimension. Consider the scalar conservation law

$$\frac{\partial \phi}{\partial t} + a\frac{\partial \phi}{\partial x} \;=\; 0, \;\; x \in \mathrm{R},\; 0 < t < T, \tag{5.1}$$

where a is a function of x and t, and T is some finite time, with the initial condition

$$\phi(x,0) = \phi_0(x), \;\; x \in \mathrm{R}. \tag{5.2}$$

Assume a uniform distribution of grid points $\{x_j : j \in \mathrm{Z}\}$ in the x direction with $x_j = jh$. The discretization of this equation using the semi-Lagrangian scheme (4.8) and (4.12) is

$$\bar{\phi}_j^{n+1} \;=\; \bar{\phi}_j^{*n}, \tag{5.3}$$

where

$$\bar{\phi}_j^{*n} \;=\; \hat{\alpha}\bar{\phi}_{j-m-1}^{n} + (1-\hat{\alpha})\bar{\phi}_{j-m}^{n}, \tag{5.4}$$

where

$$\hat{\alpha} = \alpha - m,\; \alpha = \frac{a_j^{n+1}\Delta t}{h}.$$

Here we have assumed, without loss of generality, that the departure point at time $t = t_n$ of the particle which is at the point x_j at time $t = t_{n+1}$ lies in the interval $[x_{j-m-1}, x_{j-m}]$. Note that area-weighting in one dimension involves no more than linear interpolation using the information at the two nearest grid points.

Note. If $a(x,t)$ is not constant, then the characteristic path is not a straight line. In this case an error is incurred in locating the departure point. This contributes to the overall global error of the approximation. Furthermore, if $a(x,t)$ varies rapidly in the domain $x \in \mathrm{R}$, $0 < t < T$, then it is necessary to choose Δt sufficiently small so that the computed and the actual departure points of the characteristic passing through the point x_i at time t_{n+1} lie in the same reference cell.

5.1. Stability. The stability analysis is performed in the case when a is a positive constant. If we assume that (5.3)–(5.4) has a solution of the form

$$\bar{\phi}_j^n = \bar{\phi}^0 \lambda^n \exp(ikjh), \tag{5.5}$$

then we can show that λ is given by

$$\lambda = [1 - \hat{\alpha}(1 - \exp(-ikh))] \exp(-ikmh). \tag{5.6}$$

One can show the sufficient condition for stability, i.e., $|\lambda|^2 \leq 1$, is satisfied when

$$0 \leq \hat{\alpha} \leq 1.$$

This condition is satisfied since we have chosen the interval $[x_{j-m-1}, x_{j-m}]$ so that the departure point lies in it. So the scheme is unconditionally stable.

5.2. Convergence. We define the Sobolev space $W^{2,\infty}(\mathrm{R})$ by

$$W^{2,\infty}(\mathrm{R}) = \left\{ \psi : \sup_{x \in \mathrm{R}} \left| \frac{\partial^2 \psi}{\partial x^2} \right| < \infty \right\}$$

with corresponding seminorm

$$\|\psi\|_{2,\infty} \ = \ \sup_{x \in \mathrm{R}} \left| \frac{\partial^2 \psi}{\partial x^2} \right|.$$

Similarly, we define $W^{2,\infty}(\mathrm{R} \times [0,T])$ to be the space of functions with bounded second derivatives in $\mathrm{R} \times [0,T]$. We denote by $L^\infty(0,T;W^{2,\infty}(\mathrm{R}))$ the space of functions $\psi(x,t)$ defined in $\mathrm{R} \times [0,T]$ that belong to $W^{2,\infty}(\mathrm{R})$ for any $t \in [0,T]$ and that satisfy

$$\operatorname{ess} \sup_{t \in [0,T]} \|\psi(\cdot,t)\|_{2,\infty} < \infty.$$

This space is equipped with the norm

$$\|\psi\|_{L^\infty(0,T;W^{2,\infty}(\mathrm{R}))} = \operatorname{ess} \sup_{t \in [0,T]} \|\psi(\cdot,t)\|_{2,\infty}.$$

The following convergence result is proved in Phillips and Williams [16].

THEOREM 5.1. *Let the solution of* (5.1) *belong to*

$$W^{2,\infty}(\mathrm{R} \times [0,T]) \ \cap \ L^\infty(0,T;W^{2,\infty}(\mathrm{R})),$$

and let the numerical approximation be generated by (5.3)– (5.4). *Then the error* $e_j^n = \phi(x_j,t_n) - \bar{\phi}_j^n$ *satisfies the bound*

$$\|e^n\|_\infty = O(\Delta t) + O(\min(h, h^2/\Delta t)). \tag{5.7}$$

One can deduce from this result that for some values of the discretization parameters h and Δt the error will increase as Δt is reduced up to a maximum error which is $O(\Delta t)+O(h)$. This behavior of the error as a function of the time-step Δt is in general agreement with a result of Süli and Ware [7] for the spectral method of characteristics for a similar class of problems.

6. Method of solution. The generalized Stokes problem

$$\frac{\boldsymbol{u}^{n+1} - \boldsymbol{u}^{*n}}{\Delta t} = \frac{1}{Re} \nabla^2 \boldsymbol{u}^{n+1} - \nabla p^{n+1}, \tag{6.1}$$

$$\nabla . \boldsymbol{u}^{n+1} = 0, \tag{6.2}$$

with given boundary conditions on $\boldsymbol{u}^{n+1}$ is discretized using the traditional central difference approach described earlier. Note, however, that now there will be no contribution due to convection. After the governing equations have been discretized in time and space, a suitable solution strategy must be devised to solve the resulting system of algebraic equations. One option is to solve the full problem for velocity and pressure directly at each time-step. For a large number of degrees of freedom this is a very inefficient approach. Instead we have chosen to follow the semi-implicit method for pressure linked equations (SIMPLE) methodology first advocated by Patankar and Spalding [5], which involves decoupling the velocity and pressure computations and iterating between them until convergence is reached at each time-step.

Within the SIMPLE procedure the pressure correction equation is prone to divergence unless some underrelaxation is used. The method recommended by Patankar [19] underrelaxes the velocity components in the momentum equations, with a relaxation factor α approximately equal to 0.5, and to only add a fraction of the pressure correction to the pressure, i.e.,

$$p = p^* + \alpha_p p',$$

where α_p is approximately equal to 0.8. These values for α and α_p are suggested since they have been shown to be satisfactory for a large number of flow problems. They are not necessarily the optimum values and for some problems will not produce a converged solution. It is clear that α and α_p will vary for different flow situations and may also vary for different mesh sizes within the same computational domain. Other relaxation techniques may be applied, and some of these are discussed in [23]. Clearly this algorithm is not robust. In an effort to overcome this problem Patankar [8] devised SIMPLER—SIMPLE Revised.

The argument used in the derivation of SIMPLE is that since the neighbor-point velocity corrections are removed from the velocity correction formula, the pressure correction has the sole responsibility of correcting the velocities. This leads to severe changes in the pressure correction field. Patankar [19] supposes that the pressure correction equation does a reasonable job of correcting the velocities but a poor job of correcting the pressures. The SIMPLER methodology was developed to overcome this deficiency.

To derive a pressure field equation the momentum equation is first written as

$$u_r = \frac{\sum A_{nb} u_{nb} + b_r}{A_r} + d_r(p_P - p_R). \tag{6.3}$$

We define a pseudovelocity of the form

$$\hat{u}_r = \frac{\sum A_{nb} u_{nb} + b_r}{A_r}. \tag{6.4}$$

Substitution of (6.4) into (6.3) gives

$$u_r = \hat{u}_r + d_r(p_P - p_R). \tag{6.5}$$

Similarly, we have

$$v_t = \hat{v}_t + d_t(p_P - p_T). \tag{6.6}$$

The pressure equation is derived in a similar manner to the pressure correction equation. We again integrate the continuity equation over the control volume. If

we substitute (6.5) and (6.6) into the discrete continuity equation and rearrange the terms, we obtain

$$a_P p_P = a_R p_R + a_L p_L + a_T p_T + a_B p_B + b_1 \tag{6.7}$$

with

$$a_R = d_r \Delta y, \tag{6.8}$$

$$a_L = d_l \Delta y, \tag{6.9}$$

$$a_T = d_t \Delta x, \tag{6.10}$$

$$a_B = d_b \Delta x, \tag{6.11}$$

$$a_P = a_R + a_L + a_T + a_B, \tag{6.12}$$

$$b_1 = [\hat{u}_l - \hat{u}_r]\Delta y + [\hat{v}_b - \hat{v}_t]\Delta x. \tag{6.13}$$

No approximations have been used in the derivation of the pressure equation, so if a correct velocity field is used to calculate the pseudovelocities, the pressure equation will give the correct pressure at once.

The algorithm used is based on the SIMPLER algorithm suitably ammended to incorporate the semi-Lagrangian treatment of the convection term and is described below.

The algorithm.

1. Set $n \leftarrow 0$ and define an initial velocity field $\boldsymbol{u}^{(n)}$. Put $\boldsymbol{u} \leftarrow \boldsymbol{u}^{(n)}$.
2. Calculate $u^{*(n)}$ and $v^{*(n)}$ using the semi-Lagrangian approach described in section 4.
3. Calculate pseudovelocities $\hat{u}$, $\hat{v}$ from

$$\begin{aligned} \hat{u}_r &= \tfrac{\sum A_{nb} u_{nb} + b_r}{A_r}, \\ \hat{v}_t &= \tfrac{\sum A_{nb} v_{nb} + b_t}{A_t}, \end{aligned}$$

where

$$\begin{aligned} A_r &= \textstyle\sum_{nb} A_{nb} + \frac{\Delta x \Delta y}{\Delta t}, & A_t &= \textstyle\sum_{nb} A_{nb} + \frac{\Delta x \Delta y}{\Delta t}, \\ b_r &= u_r^{*(n)} \tfrac{\Delta x \Delta y}{\Delta t}, & b_t &= v_t^{*(n)} \tfrac{\Delta x \Delta y}{\Delta t}. \end{aligned}$$

4. Solve the pressure equation for p^*

$$a_P p_P^* = a_R p_R^* + a_L p_L^* + a_T p_T^* + a_B p_B^* + b,$$

where

$$\begin{aligned} a_R &= \tfrac{(\Delta y)^2}{A_r}, & a_L &= \tfrac{(\Delta y)^2}{A_l}, \\ a_T &= \tfrac{(\Delta x)^2}{A_t}, & a_B &= \tfrac{(\Delta x)^2}{A_b}, \\ a_P &= \textstyle\sum_{nb} a_{nb}, \end{aligned}$$

and

$$b = (\hat{u}_l - \hat{u}_r)\Delta y + (\hat{v}_b - \hat{v}_t)\Delta x.$$

5. Solve the momentum equations for u', v'.

$$\begin{aligned} A_r u_r' &= \textstyle\sum_{nb} A_{nb} u_{nb}' + b_r + \Delta y (p_P^* - p_R^*), \\ A_t v_t' &= \textstyle\sum_{nb} A_{nb} v_{nb}' + b_t + \Delta x (p_P^* - p_T^*). \end{aligned}$$

6. Solve a pressure correction equation for p'

$$a_P p'_P = a_R p'_R + a_L p'_L + a_T p'_T + a_B p'_B + b,$$

where

$$b = (u'_l - u'_r)\Delta y + (v'_b - v'_t)\Delta x.$$

7. Correct the velocity field using

$$\begin{aligned} u_r &= u'_r + \tfrac{\Delta y}{A_r}(p'_P - p'_R), \\ v_t &= v'_t + \tfrac{\Delta x}{A_t}(p'_P - p'_T). \end{aligned}$$

8. Return to step 3 and repeat until convergence is obtained.
9. Set $\boldsymbol{u}^{(n+1)} \leftarrow \boldsymbol{u}$ and $n \leftarrow n+1$.
10. Return to step 2, let $\boldsymbol{u} \leftarrow \boldsymbol{u}^{(n)}$, and repeat until a steady state solution is obtained.

Note that step 2 is performed once at the beginning of each time-step and steps 3–8 take place within each time-step. Only when we have a convergent velocity solution within a time-step do we proceed to the next time-step.

7. Numerical results: Conservation law. In this section we perform a numerical experiment to illustrate the important features of the finite volume scheme developed in this paper. In this experiment we demonstrate the accuracy of this scheme by solving a problem possessing an exact solution. We consider uniform meshes only with $h = \Delta x = \Delta y$. Consider the model problem

$$\frac{\partial \phi}{\partial t} + x\frac{\partial \phi}{\partial x} - y\frac{\partial \phi}{\partial y} = 0,\ \mathbf{x} \in [1,2] \times [1,2],\ t \geq 0, \tag{7.1}$$

in which the velocity field, $\boldsymbol{u} = (x, -y)$, is divergence-free. On the two inflow boundaries we prescribe

$$\begin{aligned} \phi(1,y,t) &= 1 + y^2, \quad y \in [1,2],\ t \geq 0, \\ \phi(x,2,t) &= 1 + 4x^2, \quad x \in [1,2],\ t \geq 0. \end{aligned} \tag{7.2}$$

The initial condition is

$$\phi(x,y,0) = 0,\ x \in (1,2],\ y \in [1,2). \tag{7.3}$$

The steady state solution of this problem is

$$\phi(x,y) = 1 + (xy)^2. \tag{7.4}$$

The semi-Lagrangian algorithm is terminated when

$$\frac{\|\phi^{n+1} - \phi^n\|_\infty}{\Delta t} \leq 10^{-5}. \tag{7.5}$$

If $\tilde{\phi}_h$ denotes the converged numerical approximation to the steady state solution of the problem given by (7.4) on a grid with mesh size h, the accuracy of the discrete approximation is measured using

$$E(h) = \frac{\|\phi - \tilde{\phi}_h\|_\infty}{\|\tilde{\phi}_h\|_\infty}. \tag{7.6}$$

TABLE 2
Dependence of the error and number of iterations on mesh size with $\Delta t = 0.01$. Estimates of the order of spatial convergence are also given.

h	$\|e\|_\infty$	Iterations	p
0.25	1.013×10^{-1}	246	-
0.125	4.633×10^{-2}	182	1.13
0.0625	1.846×10^{-2}	140	1.33
0.03125	4.625×10^{-3}	111	1.36

TABLE 3
Dependence of the error on mesh size with $\Delta t = 0.001$.

h	$\|e\|_\infty$
0.25	1.088×10^{-1}
0.125	5.473×10^{-2}
0.0625	2.715×10^{-2}
0.03125	1.324×10^{-2}

In Table 2 we show how the error decays as a function of mesh size when $\Delta t = 10^{-2}$ for the scheme described in this paper. If it is assumed that the error behaves like $O(h^p)$, then the error information on two successive meshes given in Table 2 can be used to estimate the order, p, using

$$p = \frac{\ln(E(h)/E(h/2))}{\ln 2}.$$

These values are also provided in Table 2. We see that in the limit of small h the scheme is more than first-order accurate. The number of iterations required to attain the tolerance (7.5) is also given. An interesting feature is that for a given method the semi-Lagrangian algorithm converges in a fewer number of iterations as the mesh is refined. In Table 3 we show how the errors decay for a smaller time-step $\Delta t = 10^{-3}$. In all cases the errors are higher than the corresponding ones in Table 2 as predicted by the error estimate derived in Theorem 1, and the orders of spatial convergence are slightly lower. A second-order variant of the scheme has been developed for conservation laws [16]. This is based on a second-order Runge–Kutta method for determining the departure points and a second-order area-weighting scheme to ensure that the discrete conservation principle is satisfied identically.

8. Numerical results: Newtonian flow. In this section numerical calculations of laminar flow through a 2:1 contraction are presented for a range of Reynolds numbers. These calculations are compared with those generated by other authors [11], [10], [2] using different techniques. In particular, the behavior of the salient corner vortex is investigated qualitatively and quantitatively.

The work of Dennis and Smith [11] on the 2:1 contraction problem is a benchmark against which to test new and emerging numerical techniques for the Navier–Stokes equations. Their method is based on a finite difference approximation of the stream function-vorticity formulation of the governing equations. An upwind differencing scheme of Dennis and Hudson [13] is used to approximate the vorticity transport equation by adding an extra "viscous-like" term proportional to h^2. As we mentioned earlier, the standard upwind approximation is only first-order accurate. The addition of this term, known as artificial viscosity, is essential in order to obtain converged solutions for reasonably large values of Re. Without it the system of algebraic equations loses its diagonal dominance which presents convergence difficulties when solved by

iterative methods unless the mesh size is sufficiently decreased. The advantage of this upwinding scheme is that the second-order accuracy of the finite difference equations is maintained and that the artificial viscosity is applied sparingly at each grid point only if it is required. The local truncation error of the scheme is $O(h^2)$, and, therefore, it is strictly second order if $hRe << 1$. Therefore, for large values of Re small grid sizes are required for meaningful results.

Hunt [2] also uses a finite difference discretization of the stream function-vorticity formulation but on a nonuniform grid. The vorticity unknowns are eliminated to give a system solely in terms of unknown values of the stream function. There are some puzzling features of the scheme. First, when upwinding is used, the scheme fails to converge for $Re > 500$, even though one would expect the addition of a "viscous-like" term to have a stabilizing effect. Second, for a given value of Re, convergence becomes more difficult with mesh refinement.

Karageorghis and Phillips [10] use a spectral domain decomposition method to discretize the stream function formulation of the Navier–Stokes equations. The flow region is decomposed into a number of rectangular subdomains, on each of which the stream function is approximated by a truncated double Chebyshev expansion. The approximations are C^1 continuous across subregion interfaces. The nonlinear fourth-order partial differential equation for the stream function is linearized using Newton's method.

Mesh refinement is studied with reference to the size of the salient or corner vortex. This flow feature is also used as the basis of comparisons with other methods. The length of the corner vortex, L_1, is defined to be the distance between the point where the separation line meets the bottom of the channel and the salient corner. The width, L_2, of the corner vortex is defined to be the distance between the point where the separation line meets the wall parallel to the y-axis at $x = 0$ and the salient corner.

Numerical computations are performed on a series of meshes in order to ensure that the solutions obtained are independent of the mesh parameters. Both uniform and nonuniform meshes are used. The mesh parameters for the four uniform meshes (A–D) are given in Table 4. The main characteristics of the nonuniform meshes (E–G*) are given in Table 5. Meshes E–G* have mesh spacings which vary geometrically from the reentrant corner. In this way we can ensure a greater density of mesh points in the region where the solution changes most rapidly. Note that although meshes F and G contain approximately the same number of control volumes, they differ in the way the nonuniform mesh spacing varies. Mesh G is more refined around the reentrant corner than mesh F. Mesh G* corresponds to a computational domain in which the exit length is doubled from four to eight units. This extended domain allows for the examination of domain truncation effects on the numerical solution for $Re = 500$ and $Re = 1000$.

Tables 6 and 7 show the dependence of the length L_1 and the width L_2 of the salient corner vortex on the mesh. These flow characteristics are sensitive to the computational mesh. The results demonstrate that convergence with mesh refinement has been obtained over the whole range of values of the Reynolds number. The results on all the meshes were calculated with $\Delta t = 10^{-3}$. Tables 6 and 7 also show that the use of the extended domain has no appreciable effect on the values of L_1 and L_2, thus confirming that the length of the downstream channel is adequate for these computations.

Allowing $x \to \infty$ along $y = -\frac{1}{2}$, we would expect $\xi \to -12$ for a fully developed

TABLE 4
The mesh spacings and degrees of freedom for the uniform meshes A–D.

Mesh	Δx	Δy	degrees of freedom
Mesh A	$\Delta x = 0.05$	$\Delta y = 0.05$	6840
Mesh B	$\Delta x = 0.025$	$\Delta y = 0.05$	13720
Mesh C	$\Delta x = 0.05$	$\Delta y = 0.033$	10420
Mesh D	$\Delta x = 0.05$	$\Delta y = 0.025$	14000

TABLE 5
Mesh characteristics and degrees of freedom for the nonuniform meshes E–G*.

Mesh	Δx_{min}	Δy_{min}	Degrees of freedom
Mesh E	1.131×10^{-2}	2.5×10^{-2}	10800
Mesh F	1.131×10^{-2}	1.852×10^{-2}	14580
Mesh G	4.118×10^{-3}	1.512×10^{-2}	14400
Mesh G*	4.118×10^{-3}	1.512×10^{-2}	16800

flow profile at the exit. We may apply this test to check that the downstream channel is long enough for the Re numbers that we solve for. In Figures 5–7 we have plotted vorticity against downstream channel length for $Re = 1$, $Re = 100$, and $Re = 500$, respectively. These figures suggest that the downstream channel length of 4 is suitable for this range of Reynolds numbers.

The sensitivity of the computation with respect to the choice of time-step is shown in Table 8. In this table the dependence of L_1 with respect to the time-step is presented for $Re = 100$. The choice of time-step does not significantly influence the value of this characteristic of the flow problem.

The asymptotic theory of Smith [12] predicts that a separation will occur asymptotically far ahead of the step at a position $x = -L_1$, given by

$$L_1 = 0.1289 ln\, Re + D \,\text{for} Re \gg 1. \tag{8.1}$$

The constant D is of order unity, and its value depends on the contraction ratio. It is determined here by looking at the asymptotic behavior of $L_1 - 0.1289 ln\, Re$. From this analysis we obtain $D = -0.547$. In Figure 8 we plot L_1 given by (8.1) as a function of Re. On this figure we also include the values of L_1 obtained by our numerical calculations. Excellent agreement is obtained with the theoretical prediction for $Re \geq 300$. Note that the theoretical prediction is only valid for large values of the Reynolds number, although in Figure 8 it is plotted on the whole domain.

In Figures 9–14 the streamline contours are presented for Re=1, 10, 50, 100, 200, and 500, respectively, in the domain $-2 \leq x \leq 2$, $-1 \leq y \leq 0$. The salient corner vortex diminishes in size as Re increases from $Re = 1$ to $Re = 50$ and then starts to grow slowly for $Re > 50$.

In Table 9 we compare the values of L_1 obtained for different values of Re on mesh G (G* for $Re = 500,\ 1000$) with other results in the literature (Dennis and Smith [11], Hunt [2], and Karageorghis and Phillips [10]). The results of Dennis and Smith [11] have been obtained using two successive h^2-extrapolations on grids with mesh spacings of $h = \frac{1}{10}, \frac{1}{20}$ and $h = \frac{1}{40}$. The results of Hunt [2] are obtained using a transformed grid with 48×128 points and are calculated with and without the artificial viscosity term. The results of Karageorghis and Phillips are given for the most refined grid that they use with 1537 degrees of freedom.

The results in columns (a), (b), and (c) of Table 9 differ by at most 5% from each other for $1 \leq Re \leq 150$. As Re increases from 150, the values for L_1 in the first three

TABLE 6
The length, L_1, of the salient corner vortex on meshes A–G *as a function of Re.*

Re	A	B	C	D	E	F	G	G*
0				0.255	0.285	0.287	0.285	
1	0.246	0.247	0.252	0.255	0.255	0.255	0.255	
10	0.145	0.142	0.152	0.153	0.151	0.152	0.151	
50	0.118	0.123	0.122	0.122	0.122	0.123	0.122	
100	0.148	0.155	0.146	0.144	0.143	0.144	0.144	
150					0.164	0.163	0.163	
200	0.240	0.219	0.194	0.188	0.186	0.185	0.185	
300					0.223	0.222	0.223	
400					0.249	0.248	0.249	
500					0.267	0.267	0.267	0.268
1000					0.334	0.334	0.335	0.338

TABLE 7
The width, L_2, of the salient corner vortex on meshes A–G *as a function of Re.*

Re	A	B	C	D	E	F	G	G*
0					0.346	0.345	0.345	
1	0.301	0.316	0.295	0.293	0.295	0.294	0.294	
10	0.154	0.162	0.148	0.144	0.147	0.147	0.146	
50	0.114	0.127	0.109	0.106	0.109	0.110	0.110	
100	0.127	0.151	0.120	0.115	0.118	0.118	0.119	
200	0.155	0.174	0.140	0.133	0.133	0.135	0.134	
500					0.157	0.158	0.157	0.158
1000					0.174	0.173	0.173	0.175

columns of the table become closer to each other and agree to within 2%. This shows that the semi-Lagrangian scheme performs particularly well for convection dominated flows. Hunt's finite difference scheme with artificial viscosity gives results that are closer to those in the first three columns than the scheme without artificial viscosity.

In Table 10 the width, L_2, is presented for various values of Re and is compared with the values published by Dennis and Smith [11] and Hunt [2]. The values in columns (a) and (b) are within 11% of each other, although as Re increases from $Re = 50$ this percentage difference falls and for $Re = 500$ the results in columns (a) and (b) are around 1% of each other. As for the L_1 results, this would appear to show that the semi-Lagrangian scheme behaves well for high values of Re. For the schemes of Hunt [2] the values of L_2 generated are smaller than those in the first two columns for the scheme with artificial viscosity and, equivalently, larger for the scheme without artificial viscosity.

An interesting feature of the results in Tables 9 and 10 is that as Re grows from 1 to 50, both values drop so that for $Re = 50$ the value of L_1 is approximately half of its equivalent value for $Re = 1$, and the value of L_2 is approximately a third of its value for $Re = 1$. As Re increases from 50 to 1000, both the width and the length of the vortex grow but at different rates; L_1 grows more quickly than L_2. At $Re = 500$ the length L_1 is slightly larger than it was for $Re = 1$, while the value of L_2 at $Re = 500$ is still only 50% of its value at $Re = 1$. This shows that the vortex grows in size along the upstream channel more quickly than up the wall at $x = 0$ as Re increases.

The maximum values of the stream function ψ, ψ_{max}, are presented in Table 11. As we would predict from the results in Tables 9 and 10, the strength of the vortex diminishes in size between $Re = 1$ and $Re = 50$ and then grows for $50 < Re \leq 1000$.

There is no downstream recirculation region pictured in the streamline plots

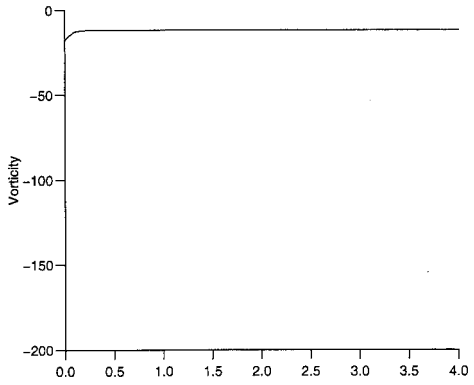

FIG. 5. *Wall vorticity* $\xi(x, -\frac{1}{2})$ *for* $x > 0$, *for* $Re = 1$.

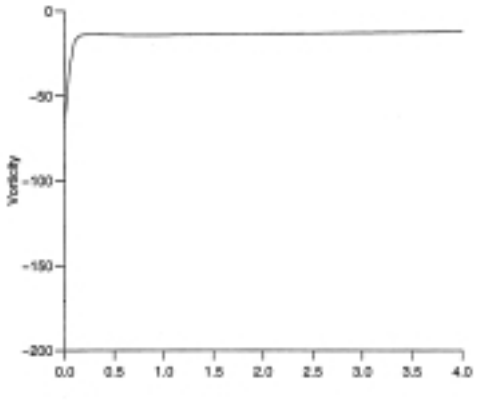

FIG. 6. *Wall vorticity* $\xi(x, -\frac{1}{2})$ *for* $x > 0$, *for* $Re = 100$.

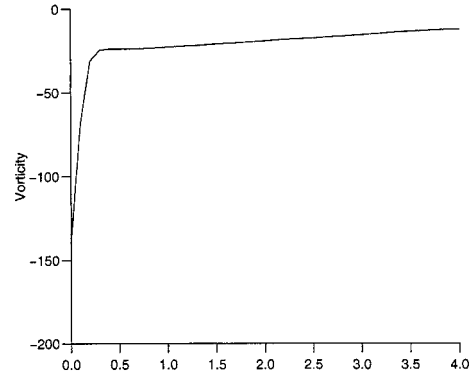

FIG. 7. *Wall vorticity* $\xi(x, -\frac{1}{2})$ *for* $x > 0$, *for* $Re = 500$.

TABLE 8
Dependence of L_1 on Δt for $Re = 100$.

Δt	L_1	L_2
10^{-3}	0.144	0.119
10^{-4}	0.145	0.121
10^{-5}	0.145	0.122

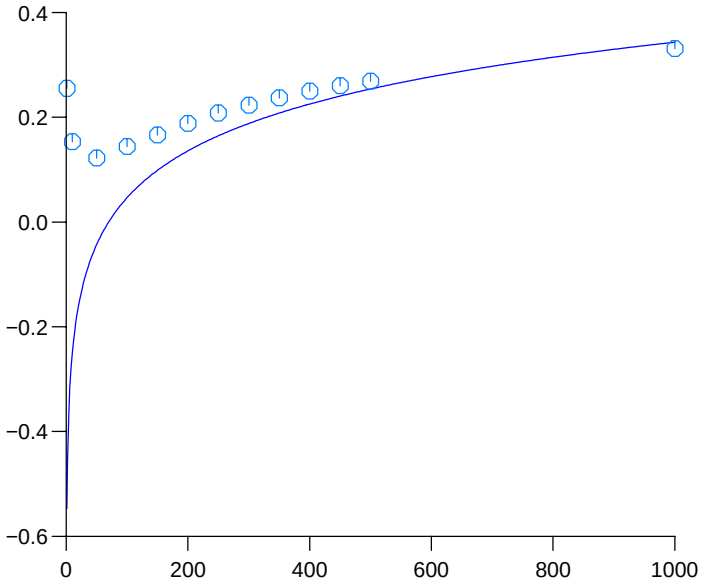

FIG. 8. *Comparison of the asymptotic predition of the value of L_1 by Smith* [12] *with the numerical results obtained in column* (a) *of Table* 9 *as a function of the Reynolds number.*

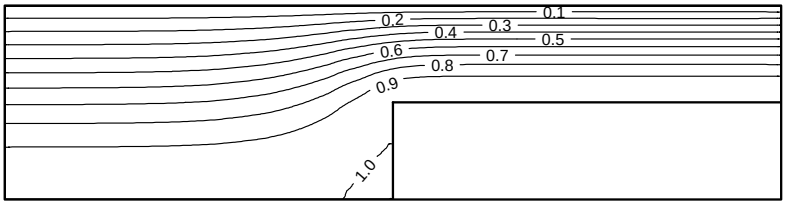

FIG. 9. *Streamlines for $Re = 1$.*

shown in Figures 9–14. However, a close examination of the values of u and v in the region of the reentrant corner indicates that for $Re \geq 100$ some recirculation may exist. For this part of the flow to be accurately resolved more work needs to be done on refining the mesh.

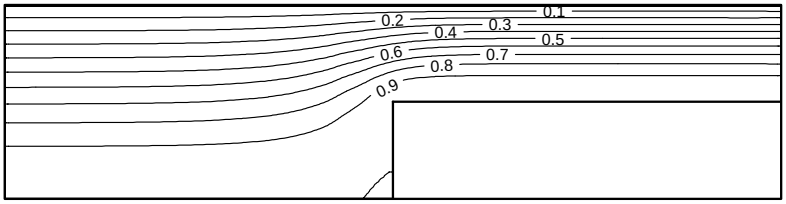

FIG. 10. *Streamlines for* $Re = 10$.

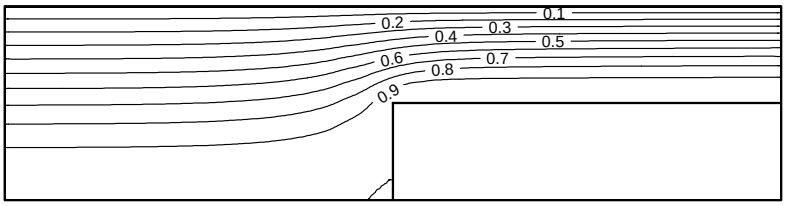

FIG. 11. *Streamlines for* $Re = 50$.

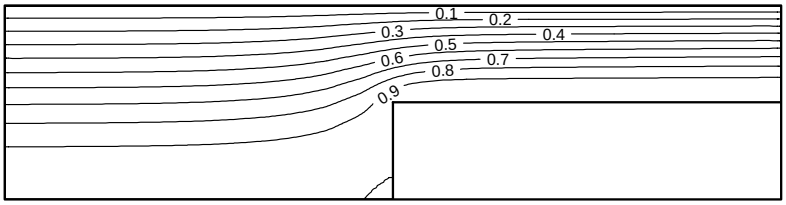

FIG. 12. *Streamlines for* $Re = 100$.

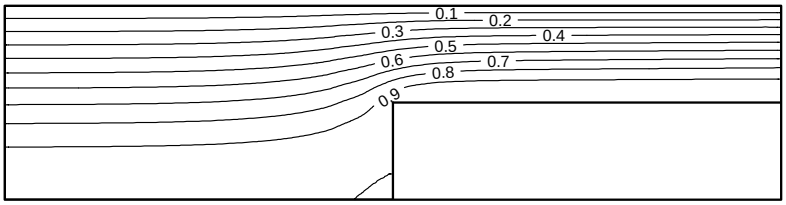

FIG. 13. *Streamlines for* $Re = 200$.

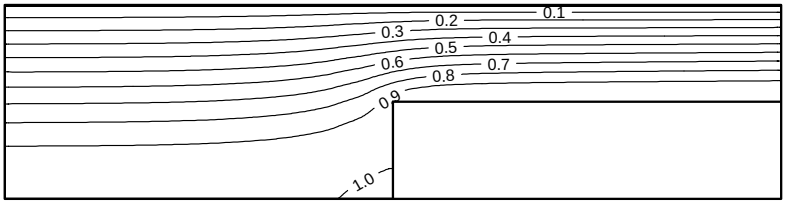

FIG. 14. *Streamlines for* $Re = 500$.

TABLE 9

The length, L_1*, of the salient corner vortex for* (a) *the semi-Lagrangian scheme,* (b) *the spectral collocation method of Karageorghis and Phillips* [10]*,* (c) *the finite-difference scheme of Dennis and Smith* [11]*,* (d) *the finite-difference scheme of Hunt* [2] *without artificial viscosity, and* (e) *the finite-difference scheme of Hunt* [2] *with artificial viscosity.*

Re	(a)	(b)	(c)	(d)	(e)
1	0.255	-	0.255	-	-
10	0.151	0.148	0.155	-	-
50	0.122	0.123	0.129	-	-
100	0.144	0.140	0.144	-	-
150	0.163	0.155	-	-	-
200	0.185	0.183	-	-	-
250	0.208	0.205	-	0.227	0.209
300	0.223	0.223	-	-	-
350	0.237	0.233	-	-	-
400	0.249	0.244	-	-	-
450	0.260	0.255	-	-	-
500	0.268	0.265	0.266	0.308	0.260
1000	0.338	-	0.341	0.394	-

TABLE 10

The width, L_2*, of the salient corner vortex for* (a) *the semi-Lagrangian scheme,* (b) *the finite-difference scheme of Dennis and Smith* [11]*,* (c) *the finite-difference scheme of Hunt* [2] *without artificial viscosity, and* (d) *the finite-difference scheme of Hunt* [2] *with artificial viscosity.*

Re	(a)	(b)	(c)	(d)
1	0.294	0.303	-	-
10	0.146	0.160	-	-
50	0.110	0.122	-	-
100	0.119	0.125	-	-
500	0.158	0.159	0.164	0.149
1000	0.175	0.177	0.188	-

9. Concluding remarks. A semi-Lagrangian finite volume method for solving the time-dependent incompressible Navier–Stokes equations is presented. A time-splitting scheme is used to decouple the treatment of convection from the solution of a generalized Stokes problem. The convection problem is solved using a semi-Lagrangian approach in which the vertices of a control volume at the new time level are traced back in time over a time-step using a particle following transformation. The values of the velocity components in the transformed control volumes at the previous time level are determined using an area-weighting technique which ensures

TABLE 11
The maximum value of the streamfunction, ψ, of the salient corner vortex.

Re	ψ_{max}
1	1.00047
10	1.00009
50	1.00007
100	1.00010
500	1.00054
1000	1.00109

that the conservation property enjoyed by the pure convection problem is satisfied indentically by construction. This approach circumvents problems associated with upwind biased schemes. The generalized Stokes problem is solved using the standard SIMPLER method. The scheme is applied to the flow through a 2:1 contraction and is demonstrated to be robust and accurate. Comparisons are made with other published work on this problem and excellent agreement is found.

Future work will concentrate on developing higher-order methods in time for integrating along the particle paths. The extension of this technique to problems in computational rheology is currently in progress [14, 15].

Acknowledgment. The second author would like to thank the United Kingdom Engineering and Physical Science Research Council for financial support in the form of a research studentship.

REFERENCES

[1] C. HIRSCH, *Numerical Computation of Internal and External Flows. Vol.* 2: *Computational Methods for Inviscid and Viscous Flows*, John Wiley, Chichester, UK, 1990.
[2] R. HUNT, *The numerical solution of the laminar flow in a constricted channel at moderately high Reynolds number using Newton iteration*, Internat. J. Numer. Methods Fluids, 11 (1990), pp. 247–259.
[3] K. W. MORTON, A. PRIESTLEY, AND E. SÜLI, *Stability analysis of the Lagrange–Galerkin method with nonexact integration*, RAIRO Modél. Math. Anal. Numér., 22 (1988), pp. 625–653.
[4] J. S. SCROGGS AND F. H. M. SEMAZZI, *A conservative semi-Lagrangian method for multidimensional fluid dynamics applications*, Numer. Methods Partial Differential Equations, 11 (1995), pp. 445–452.
[5] S. V. PATANKAR AND D. B. SPALDING, *A calculation procedure for heat, mass and momentum transfer in three dimensional parabolic flows*, Int. J. Heat Mass Transfer, 15 (1972), pp. 1787–1806.
[6] B. P. LEONARD, *A stable and accurate convection modelling procedure based on quadratic upstream interpolation*, Comput. Methods Appl. Mech. Engrg., 15 (1979), pp. 59–98.
[7] E. SÜLI AND A. WARE, *A spectral method of characteristics for hyperbolic problems*, SIAM J. Numer. Anal., 28 (1991), pp. 423–445.
[8] S. V. PATANKAR, *A calculation procedure for two-dimensional elliptic situations*, Numer. Heat Transfer, 4 (1981), pp. 409–425.
[9] P. H. GASKELL AND A. K. C. LAU, *Curvature-compensated convective transport: SMART, a new boundedness-preserving transport algorithm*, Internat. J. Numer. Methods Fluids, 8 (1988), pp. 617–641.
[10] A. KARAGEORGHIS AND T. N. PHILLIPS, *Conforming Chebyshev spectral methods for the solution of laminar flow in a constricted channel*, IMA J. Numer. Anal, 11 (1991), pp. 33–54.
[11] S. C. R. DENNIS AND F. T. SMITH, *Steady flow through a channel with a symmetrical constriction in the form of a step*, Proc. Roy. Soc. London A, 372 (1980), pp. 393–414.
[12] F. T. SMITH, *The separating flow through a severely constricted symmetric tube*, J. Fluid Mech., 90 (1979), pp. 725–754.

[13] S. C. R. Dennis and J. D. Hudson, *A difference method for solving the Navier–Stokes equations*, in Proceedings of the First Conference on Numerical Methods in Laminar and Turbulent Flow, Pentech Press, London, 1978.

[14] T. N. Phillips and A. J. Williams, *Semi-Lagrangian finite volume method for viscoelastic flow problems*, in The Mathematics of Finite Elements and Applications X, J. R. Whitman, ed., Elsevier, Amsterdam, 2000, pp. 335–344.

[15] T. N. Phillips and A. J. Williams, *A semi-Lagrangian finite volume method for solving viscoelastic flow problems*, in Proceedings of the Fifth European Rheology Conference, I. Emri and R. Cvelbar, eds., Steinkopff, Portorož, Slovenia, 1998, pp. 299–300.

[16] T. N. Phillips and A. J. Williams, *Conservative semi-Lagrangian finite volume schemes*, Numer. Methods Partial Differential Equations, to appear, 2001.

[17] A. J. Williams, *A Semi-Lagrangian Finite Volume Method for Incompressible Fluid Flow*, Ph.D. thesis, University of Wales, Aberystwyth, UK, 1998.

[18] R. J. LeVeque, *Numerical Methods for Conservation Laws*, 2nd ed., Lectures in Mathematics ETH, Zürich, Birkhauser Verlag, Basel, 1992.

[19] S. V. Patankar, *Numerical Heat Transfer and Fluid Flow*, Hemisphere, New York, 1981.

[20] R. W. Hockney and J. W. Eastwood, *Computer simulation using particles*, Math. Comput., McGraw-Hill, New York, 1981.

[21] F. H. Harlow, *The Particle in Cell Computing Method for Fluid Dynamics*, Methods Comput. Phys. 3, B. Adler, S. Fernbach, and M. Rotenberg, eds., Academic Press, New York, 1964.

[22] O. Pironneau, *On the transport-diffusion algorithm and its applications to the Navier–Stokes equations*, Numer. Math., 38 (1982), pp. 309–332.

[23] J. P. Van Doormal and G. D. Raithby, *Enhancements of the SIMPLE method for predicting incompressible fluid flows*, Numer. Heat Transfer, 7 (1984), pp. 147–163.

[24] J. R. Manson and S. G. Wallis, *Accuracy characteristics of traditional finite volume discretizations for unsteady computational fluid dynamics*, J. Comput. Phys., 132 (1997), pp. 149–153.

[25] J. R. Manson and S. G. Wallis, *Accurate numerical simulation of advection using large time steps*, Internat. J. Numer. Methods Fluids, 24 (1997), pp. 127–139.